Inorg. Chem. **2006**, *45*, 6276–6281

Two Cobalt(II) 5-Aminoisophthalate Complexes and Their Stable Supramolecular Microporous Frameworks

En Tang,[†] Yu-Mei Dai,[†,‡] Jian Zhang,[†] Zhao-Ji Li,[†] Yuan-Gen Yao,*[,†] Jie Zhang,*[,†] and Xu-Dong Huang[§]

State Key Laboratory of Structural Chemistry, Fujian Institute of Research on the Structure of Matter, The Chinese Academy of Sciences, Fuzhou, Fujian 350002, P. R. China, College of Chemistry & Material Science, Fujian Normal University, Fuzhou, Fujian 350007, P. R. China, and Genetics & Aging Research Unit, Massachusetts Institute of Neurodegenerative Diseases and Department of Psychiatry, Massachusetts General Hospital and Harvard Medical School, Charlestown, Massachusetts 02129

Received February 9, 2006

Two stable supramolecular microporous cobalt(II) polymers, namely $[Co(HAIP)_2]_n \cdot 3nH_2O$ (**1**) and $[Co(AIP)(H_2O)]_n$ (**2**), AIP = 5-aminoisophthalate, were hydrothermally synthesized and characterized by single-crystal X-ray diffraction, IR spectra, thermogravimetric analyses, and variable-temperature magnetic susceptibility measurements. The two complexes are constructed from the same $Co_2(CO_2)_2$ SBU, which is extended into a 1D chain in **1** and a 2D layer in **2**. As a result, **1** and **2** are 2D and 3D coordination polymers, respectively. The 3D supramolecular network of complex **1** is held up by strong hydrogen bonds formed between carboxylate groups and shows very high stability when the free H_2O molecules are removed, indicating an extraordinarily stable H-bonding system. Upon water ligands being liberated, complex **2** becomes a stable microporous solid with coordination-unsaturated Co centers. The behavior of the susceptibility curve of **1** suggests the occurrence of an interesting intrachain antiferromagnetic coupling between the Co(II) ions and the presence of a significant orbital contribution, whereas the features of **2** indicate an antiferromagnetic coupling with $T_N = 3.5$ K and a long-range antiferromagnetic order with a field-induced magnetic transition.

Introduction

The current interest focused on the crystal engineering of coordination polymeric frameworks stems not only from their potential application as new functional solid materials[1,2] but also from their intriguing architectures and topologies.[3,4] One of the most effective approaches to obtain polymeric frameworks is hydro(solvo)thermal assembly by incorporating appropriate metal ions (connectors) with multifunctional bridging ligands (linkers).[5] However, the hydro(solvo)thermal reaction is highly influenced by many factors, such as the oxidation state and coordination geometry of the metal center, temperature, pH value, metal-to-ligand ratio, ligands, solvents, and counterions. In many cases, a subtle alteration in any of these factors can lead to totally different products. A great deal of work on hydro(solvo)thermal synthesis with N-donor rigid heteroaromatic ligands, such as pyridinecarboxylate or 4,4′-bipyridine, has already been reported.[6,7] However, there has been relatively little effort on the transition metal amino benzoate polymers, mainly because

* To whom correspondence should be addressed. E-mail: yyg@fjirsm.ac.cn (Y.-G.Y.). Fax: (86)-591-83714946.

[†] Fujian Institute of Research on the Structure of Matter, The Chinese Academy of Sciences.

[‡] Fujian Normal University.

[§] Massachusetts General Hospital and Harvard Medical School.

(1) (a) Sato, O.; Iyoda, T.; Fujishima, A.; Hashimoto, K. *Science* **1996**, *271*, 49. (b) Kahn, O.; Martinez, C. *Science* **1998**, *279*, 44.

(2) (a) Evans, O. R.; Xiong, R.; Wang, Z.; Wong, G. K.; Lin, W. *Angew. Chem., Int. Ed.* **1999**, *38*, 536. (b) Fujita, M.; Kwon, Y. J.; Washizu, S.; Ogura, K. *J. Am. Chem. Soc.* **1994**, *116*, 1151.

(3) (a) Hagrman, P. J.; Hagrman, D.; Zubieta, J. *Angew. Chem., Int. Ed.* **1999**, *38*, 2639. (b) Yaghi, O. M.; Li, H.; Davis, C.; Richardson, D.; Groy, T. L. *Acc. Chem. Res.* **1998**, *31*, 474.

(4) (a) Blake, A. J.; Champness, N. R.; Hubberstey, P.; Li, W. S.; Withersby, M. A.; Schroer. M. *Coord. Chem. Rev.* **1999**, *183*, 117. (b) Dai, Y. M.; Ma, E.; Tang, E.; Zhang, J.; Li, Z. J.; Huang, X. D.; Yao, Y. G. *Cryst. Growth Des.* **2005**, *5*, 1313.

(5) (a) Moulton, B.; Zaworotko, M. J. *Chem. Rev.* **2001**, *101*, 1629. (b) Batten, S. R.; Robson, R. *Angew. Chem., Int. Ed.* **1998**, *37*, 1460. (c) Hagman, P. J.; Hagman, D.; Zubieta, J. *Angew. Chem., Int. Ed.* **1999**, *38*, 2638.

(6) Wang, Z. M.; Zhang, B.; Kurmoo, M.; Green, M. A.; Fujiwara, H.; Otsuka, T.; Kobayashi, H. *Inorg. Chem.* **2005**, *44*, 1230−1237.

(7) Wang, Z. M.; Zhang, B.; Fujiwara, H.; Kobayashi, H.; Kurmoo, M. *Chem. Commun*. **2004**, 416.

10.1021/ic0602244 CCC: $33.50
Published on Web 07/11/2006

of the more flexible coordination manner of the amino group under hydro(solvo)thermal conditions.

Meanwhile, one of the challenges in microporous coordination polymeric frameworks is their fragility. Unlike their inorganic analogues, which are held together with rugged covalent bonds, coordination polymeric molecules are always glued with relatively weak coordination or supramolecular interactions. Although numerous coordination networks with interesting structural aspects have been reported,[8,9] the porous metal−organic coordination networks extended via hydrogen bonds often show poor thermal stability. Stable networks sustained by hydrogen-bond interactions are still rare or lacking.[10] To explore new microporous and magnetic materials,[11−15] our current research has focused on the synthesis of highly stable microporous open frameworks, especially those held up by hydrogen-bond interactions.

Herein, we report the crystal structures and magnetic properties of two highly stable 3D cobalt(II) supramolecular polymers, $[Co(HAIP)_2]_n \cdot 3nH_2O$ (**1**) and $[Co(AIP)H_2O]_n$ (**2**), AIP = 5-aminoisophthalate, which were prepared by the hydrothermal reaction of $CoSO_4 \cdot 7H_2O$ with H_2AIP under different pH conditions. The strong hydrogen-bond interactions extend complex **1** into a 3D open supramolecular architecture, and it exhibits extraordinarily high stability. In **2**, Co(II) cations link AIP ligands to yield a 3D network containing microporous channels viewed along the *c* axis, which are filled by coordinated water molecules. Thermogravimetric studies show the microporous channels could contain open metal sites when coordination water molecules are eliminated.

Experimental Section

General. All chemicals and reagents are commercially available and were used as received without further purification. Infrared spectra (KBr pellets) were recorded in the range of 400−4000 cm^{-1} on a Nicolet Magna 750 FT-IR spectrometer. The C, H, and N microanalyses were recorded on an Elemental Vario EL III elemental analyzer. Thermogravimetric analyses (TGA) were performed on a Mettler Toledo TGA 851e analyzer under nitrogen with a heating rate of 10 °C min^{-1}. Powder X-ray diffraction (XRD) data were obtained using a Philips X'Pert-MPD diffractometer with Cu Kα radiation (λ = 1.54056 Å). Variable-temperature magnetic susceptibility and magnetization measurements were performed on a Maglab System 2000 magnetometer. The experimental susceptibilities were corrected for the diamagnetism of constituent atoms.

Synthesis of $[Co(C_8NH_6O_4)_2]_n \cdot 3nH_2O$ (1). A mixture of $CoSO_4 \cdot 7H_2O$ (1.0 mmol), H_2AIP (1.00 mmol), C_2H_5OH (2 mL), and H_2O (15 mL) was sealed in a Teflon-lined stainless steel vessel and heated at 433 K for 3 days under autogenous pressure. Deep red crystals were produced when the mixture was slowly cooled to room temperature (yield: 60%, on the basis of Co). Anal. Calcd for $C_{16}H_{18}CoN_2O_{11}$: C, 40.61; H, 3.83; N, 5.92. Found: C, 40.58; H, 3.77; N, 5.90. IR (KBr pellet, cm^{-1}): 3312 (vs), 3272 (vs), 1683 (s), 1605 (s), 1475 (vs), 1396 (s), 1331 (s), 1256 (vs), 963 (vs), 769 (vs), 513 (w).

Synthesis of $[Co(C_8NH_5O_4)(H_2O)]_n$ (2). The pH value of a mixture of $CoSO_4 \cdot 7H_2O$ (0.50 mmol), AIP (1.00 mmol), C_2H_5OH (5 mL), and H_2O (5 mL) was adjusted to 7.5 by 10% KOH under vigorous stirring. The mixture was sealed in a Teflon-lined stainless steel vessel and heated at 433 K for 3 days under autogenous pressure. Deep red crystals were produced when the mixture was slowly cooled to room temperature (yield: 48%, on the basis of Co). Anal. Calcd for $C_8H_7CoNO_5$: C, 37.52; H, 2.76; N, 5.47. Found: C, 37.48; H, 2.70; N, 5.42. IR (KBr pellet, cm^{-1}): 3354 (s), 3173 (s), 1682 (vs), 1539 (vs), 1466 (vs), 1162 (w), 720 (w).

Crystallographic Measurements. All of the diffraction data were collected on a Siemens SMART CCD diffractometer with graphite-monochromated Mo Kα radiation (λ = 0.71073 Å) at a temperature of 293(2) K, using the $\omega-2\theta$ scan technique ($1.61° < \theta < 25.02°$). The intensity data were corrected by Lp factors and empirical absorption. The structure was solved by direct methods and refined by full-matrix least-squares techniques on F^2 using SHELXTL-97.[16] The non-hydrogen atoms were refined anisotropically, and the hydrogen atoms on carbon atoms and those of amido as well as carboxyl were added according to theoretical models; the hydrogen atoms of O1W and O2W were positioned geometrically. Crystal data and details of the structure determination are summarized in Table 1, and the selected bond lengths and angles for the two complexes are given in Table 2.

Table 1. Collected Crystallographic Data and Parameters for **1** and **2**

	1	**2**
formula	$C_{16}H_{18}CoN_2O_{11}$	$C_8H_7CoNO_5$
M_r	473.25	256.08
cryst syst	monoclinic	monoclinic
space group	*C*2/*c*	*P*2(1)/*c*
a (Å)	28.4110(9)	8.835(4)
b (Å)	4.4718(2)	12.519(5)
c (Å)	15.3333(6)	7.908(3)
β (deg)	116.852(2)	97.532(4)
V (Å^3)	1738.02(12)	867.1(6)
Z	4	4
D_{calcd} (mg cm^{-3})	1.809	1.962
μ (mm^{-1})	1.059	1.978
range for data collection	2537	6571
no. of independent reflns	1538	1991
final R1, wR2 [$I > 2\sigma(I)$]	0.0432, 0.1202	0.0343, 0.0844
R1, wR2 indices (all data)	0.0475, 0.1266	0.0373, 0.0865

Results and Discussion

Crystal Structures of $[Co(C_8NH_6O_4)_2]_n \cdot 3nH_2O$ (1). Single-crystal X-ray diffraction study reveals that **1** has a porous 3D supramolecular network linked by both coordinating and hydrogen bonds. As illustrated in Figure 1, the Co(II) atom is located in the elongated octahedral environment: four oxygen atoms from four different AIP ligands in the equatorial plane and two N atoms from two different AIP ligands in the apical positions. The AIP ligand in **1** uses one of its two carboxylate groups to bidentate two cobalt-

(8) Li, H.; Eddaoudi, M.; O'Keeffe, M.; Yaghi, O. M. *Nature* **1999**, *402*, 276.
(9) (a) Gutschke, S. O. H.; Molinier, M.; Powell, A. K.; Wood, P. T. *Angew. Chem., Int., Ed.* **1997**, *38*, 991. (b) Brunet, P.; Simard, M.; Wuest, J. D. *J. Am. Chem. Soc.* **1997**, *119*, 2737.
(10) (a) Cheng, D.; Khan, M. A.; Houser, R. P. *Inorg. Chem.* **2001**, *40*, 6858. (b) Choi, H. J.; Suh, M. P. *Inorg. Chem.* **1999**, *38*, 6309.
(11) Beauvais, L. G.; Long, J. R. *J. Am. Chem. Soc.* **2002**, *124*, 12096.
(12) Pan, L.; Ching, N.; Huang, X.-Y.; Li, J. *Inorg. Chem.* **2000**, *39*, 5333.
(13) Huang, Z.-L.; Drillon, M.; Masciocchi, N.; Sironi, A.; Zhao, J.-T.; Rabu, P.; Panissod, P. *Chem. Mater.* **2000**, *12*, 2805.
(14) Fujita, M.; Kwon, Y. J.; Washizu, S.; Ogura, K. *J. Am. Chem. Soc.* **1994**, *116*, 1151.
(15) Eddaoudi, M.; Kim, J.; Rosi, N.; Vodak, D.; Wachter, J.; O'Keeffe; M.; Yaghi, O. M. *Science* **2002**, *295*, 469.
(16) Sheldrick, G. M. *SHELXTL-97, Program for Crystal Structure Refinement*; University of Göttingen: Göttingen, Germanny, 1997.

Table 2. Selected Bond Lengths (Å) and Angles (deg) for **1** and **2**[a]

		Complex **1**	
Co(1)−O(3)#1	2.088(2)	O(3)#1−Co(1)−O(3)#2	180.00(1)
Co(1)−O(3)#2	2.088(2)	O(3)#1−Co(1)−O(4)#3	92.44(9)
Co(1)−O(4)#3	2.097(2)	O(3)#1−Co(1)−O(4)#4	87.56(9)
Co(1)−O(4)#4	2.097(2)	O(3)#1−Co(1)−N(1)	87.31(10)
Co−N(1)	2.215(3)	O(4)#3−Co(1)−N(1)	90.57(9)
Co(1)−N(1)#5	2.215(3)		
		Complex **2**	
Co(1)−O(1)#1	1.9928(2)	O(1)#1−Co(1)−O(2)	108.67(8)
Co(1)−O(2)	2.0180(2)	O(1)#1−Co(1)−O(1W)	88.43(7)
Co(1)−O(1W)	2.0980(2)	O(2)−Co(1)−O(1W)	90.58(7)
Co(1)−O(4)#2	2.1228(2)	O(1)#1−Co(1)−O(4)#2	155.86(7)
Co(1)−N(1)#3	2.220(2)	O(2)−Co(1)−O(4)#2	95.45(7)
Co(1)−O(3)#2	2.2485(2)	O(1W)−Co(1)−O(4)#2	90.20(7)

[a] Symmetry transformations used to generate equivalent atoms: For **1**: #1 $x, -y+1, z+1/2$ #2 $-x+1/2, y-1/2, -z+1/2$ #3 $-x+1/2, y+1/2, -z+1/2$ #4 $x, -y, z+1/2$ #5 $-x+1/2, -y+1/2, -z+1$. For **2**: #1 $-x+1, -y+1, -z$ #2 $-x+2, y-1/2, -z+1/2$ #3 $x, -y+3/2, z+1/2$ #4 $-x+2, y+1/2, -z+1/2$.

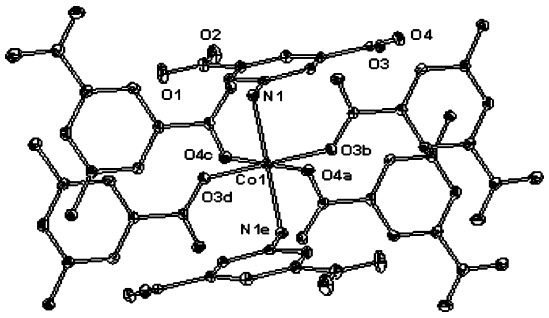

Figure 1. View of the coordination environment of Co in **1** (a: $1/2-x, 1/2+y, 1/2-z$; b: $1/2-x, -1/2+y, 1/2-z$; c: $x, -y, 1/2+z$, d: $x, 1-y, 1/2+z$, e: $1/2-x, 1/2-y, 1-z$).

(II) atoms, whereas the other carboxylate group does not participate in coordination to the Co(II) center. The amino group of AIP coordinates to the third cobalt(II) atom.

The secondary building unit (SBU) of **1** is a dicobalt dicarboxylate $Co_2(CO_2)_2$, in which the two Co atoms, separated by 4.472 Å, are bridged by two μ_2-bridging carboxylate groups. The $Co_2(CO_2)_2$ SUBs are lined up into a 1D chain along the *b* axis by sharing the Co(II) atom. This 1D chain is further linked by two N atoms from two adjacent chains into a 2D layer propagating along the *bc* plane. It is noteworthy that one of the two carboxylate groups of each AIP ligand does not participate in the coordination, but acts as a hydrogen-bond acceptor and donor. As shown in Figure 2b, there exist strong hydrogen bonds between two carboxylate groups from two different AIP ligands (O···O = 2.598(4) Å, O−H···O = 162(10)°). The hydrogen bonds pillar the layers into a 3D supramolecular open framework with a pore along the *a* axis (approximate dimensions 7.9×13 Å^2), which is occupied by free and removable water molecules.

Crystal Structures of $[Co(C_8NH_5O_4)(H_2O)]_n$ (2). The X-ray diffraction analysis reveals that complex **2** exhibits a 3D metal−organic framework. As shown in Figure 3, the asymmetric unit contains one Co atom, one AIP ligand, and one coordinated water molecule. All the equivalent Co(II) atoms are coordinated by four oxygen atoms and one N atom from four different AIP ligands, as well as one H_2O. Each AIP ligand employs its carboxylate groups and amino group in turn to coordinate to four Co(II) centers. Different from

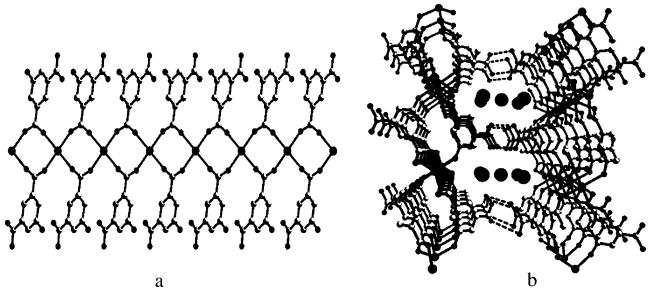

Figure 2. (a) One-dimensional $Co_2(CO_2)_2$ chain in **1**, Co···Co separated by 4.472 Å. (b) Three-dimensional open supramolecular architecture pillared by strong hydrogen bonds. The pores are occupied by free water molecules represented by magnified red balls for clarity.

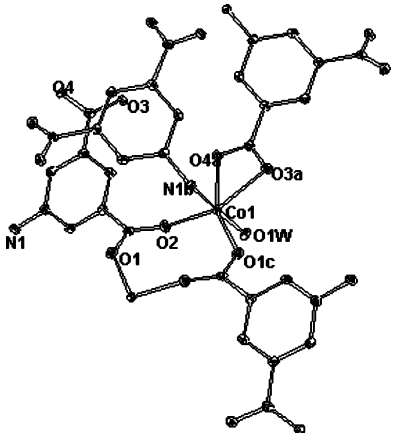

Figure 3. View of the coordination environment of Co in **2** (a: $2-x, -1/2+y, 1/2-z$; b: $x, 3/2-y, 1/2+z$; C: $1-x, 1-y, -z$).

the coordination model in **1**, the coordination modes of AIP ligands in **2** can be described as follows: one of its two carboxylate groups, acting as a bidentate ligand, bridges two Co(II) centers and the other one coordinates to a third Co(II) center as bidentate, whereas the amino group bonds to the fourth Co(II) center. The secondary building unit (SBU) of **2** is also a dicobalt dicarboxylate SBU $Co_2(CO_2)_2$, with a Co···Co distance 4.3 Å. If we omit Co−N bonds, the binuclear subunits are interconnected through Co−O bonds into a 2D layer (Figure 4a). The 2D layers are assembled into an unprecedented 3D framework via Co−N bonds. As a contrast to complex **1**, the H_2O molecule in **2** is not free but coordinated to a Co(II) center. If we omit H_2O molecules in **2,** a pore with the dimensions of ca. 7×6 Å^2 is observed along the *c* axis. Two water molecules, acting as the disguise guests, are filled inside the void of the pore. Because the metal−AIP coordination bonds are much stronger than the metal−water bonds, it is expected that water liberation by heating will facilitate complex **2** into a coordination-unsaturated microporous complex. The coordination-unsaturated metal site can consequently serve as the binding site to other inclusions.[17,18]

If we take the binuclear SBU to be a single node, such a SBU becomes a 6-connected node, and each AIP^{2-} ligand can be regarded as a three-connected vertex that links three

(17) (a) Yaghi, O. M.; Li, H. L.; Groy, T. L. *J. Am. Chem. Soc.* **1996**, *118*, 9096−9101.
(18) Copp, S. B.; Subramanian, S.; Zaworotko, M. J. *Angew. Chem., Int. Ed.* **1993**, *32*, 706−709.

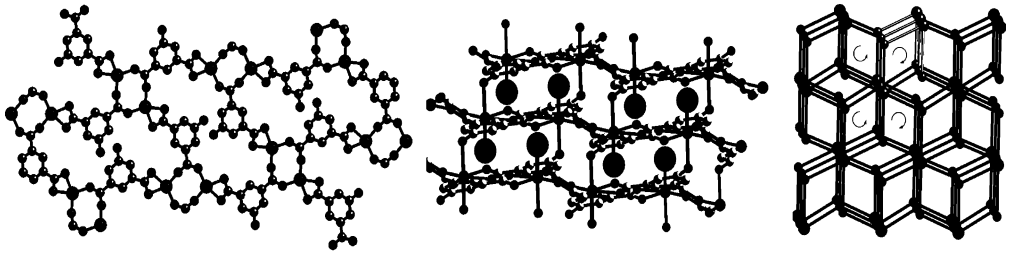

Figure 4. (a) Two-dimensional layer generated from the binuclear SBU via Co−O bonds. (b) Three-dimensional stacking structure of **2** where the H_2O ligands are represented by magnified red balls for clarity. (c) Topological representation of **2**.

SBUs. The linkage of three- and six-connected vertexes is illustrated in Figure 4c. This framework is a distorted (3, 6)-connected net with the Schläfli symbol being $(4.6^2)_2$-$(4^2.6^{10}.8^3)$, but it is obviously different from the other reported (3, 6)-connected net of the same Schläfli symbol (such as rutile (rtl) or sit net).[19] An interesting feature of this net is the presence of parallel single helices running through the structure, as highlighted in Figure 4c. The six-connected nodes act as hinges of four 2_1 helices with equal handedness, whereas the three-connected nodes act as hinges of two edge-sharing 2_1 helices with different handedness. As an overall effect, these connections make the net racemic.

IR Spectra. The IR spectra of **1** and **2** show the characteristic bands of the AIP ligand between 1630 and 1460 cm^{-1} for the asymmetric vibration and between 1441 and 1367 cm^{-1} for the symmetric vibration, and the broad bands of water between 3215 and 3442 cm^{-1}. The characteristic bands at 1684 cm^{-1} in **1** are attributed to the protonated carboxylate groups of AIP. In **2**, the absence of the expected characteristic bands at 1730−1680 cm^{-1}, which are attributed to the protonated carboxylate group, indicate the complete deprotonation of AIP in **2**.[20] The respective values of $[\nu_{asym}(CO_2)-\nu_{sym}(CO_2)]$ clearly indicate the presence of a bridging mode (162 cm^{-1}) in complex **1** and both the chelating mode (79 cm^{-1}) and bridging mode (130 cm^{-1}) in complex **2**.[21] These results are consistent with that of the X-ray analysis.

Thermogravimetric Studies and X-ray Powder Diffraction. The thermogravimetric analysis (TGA) of complex **1** reveals that there are three stages of weight loss in the temperature range of 30−600 °C (Figure 5). The first stage, occurring between 30 and 90 °C, is attributed to the loss of three uncoordinated water molecules per formula (observed weight loss, 10.6%; calcd, 11.4%). The weight is almost unchanged in the second stage in a very long temperature range (90−375 °C). Above 375 °C, the product begins to decompose. The TGA curve of the free AIP ligand shows that it decomposes at 303 °C. This means that complex **1** is more stable than the free AIP ligand, and the H bonds between these two carboxylic groups are strong enough to withstand the high temperature of 375 °C.

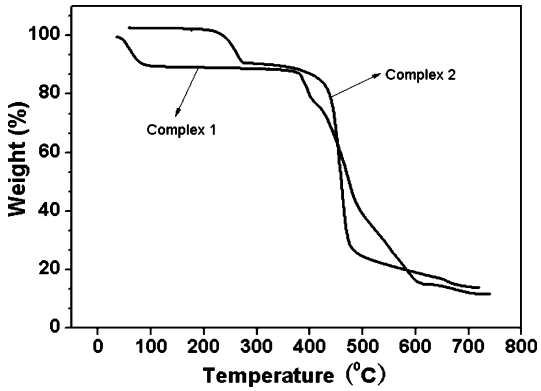

Figure 5. TGA plots of complexes **1** and **2**.

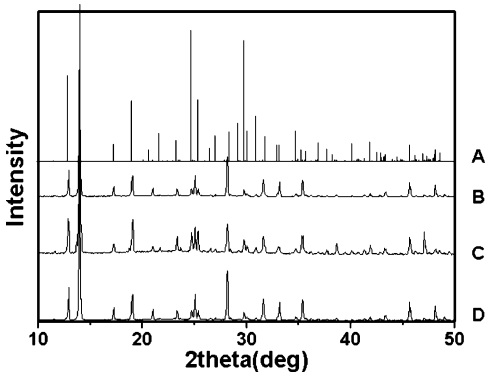

Figure 6. XPRD patterns for **1**: (A) the simulated pattern, (B) taken at room temperature, (C) after heating at 130 °C for 2 h, and (D) after heating at 350 °C for 2 h.

To examine the porous properties of the materials, we heated the synthesized crystal samples of **1** at 130 and 350 °C for 2 h; the position of the most intensive line remain unchanged relative to that of the single crystal (Figure 6), which shows us the extraordinary thermal stability relies on the hydrogen-bonding interactions. **1** also exhibits the ability to absorb water expediently in this process when exposed in atmosphere, indicating a reversible process; thus, **1** can be envisaged as a good candidate for a new molecular sieve.[22]

The TGA analysis for **2** showed the following two strikingly clean and well-separated weight-loss steps. In the first region (30−260 °C), it lost coordinated water molecules (8% observed, 7% calcd). On further heating, **2** lost weight continuously, corresponding to preliminary decomposition at 370 °C and fast decomposition around 480 °C. The synthesized crystal samples of **2** were heated at 350 °C for

(19) Blatov, V. A.; Carlucci, L.; Ciani, G.; Proserpio, D. M. *CrystEngComm* **2004**, *6*(*65*), 377−395.
(20) Bellamy, L. J. *The Infrared Spectra of Complex Molecules*; Wiley: New York, 1958.
(21) (a) Deacon, G. B.; Phillips, R. J.*Coord. Chem. Rev.* **1980**, *33*, 227. (b) Nakamoto, K. *Infrared Spectra and Raman Spectra of Inorganic and Coordination Compounds*; John Wiley & Sons: New York, 1986.
(22) Breck, D. W. *Zeolite Molecular Sieves, Structure, Chemistry, and Use*; John Wiley & Sons: New York, 1974.

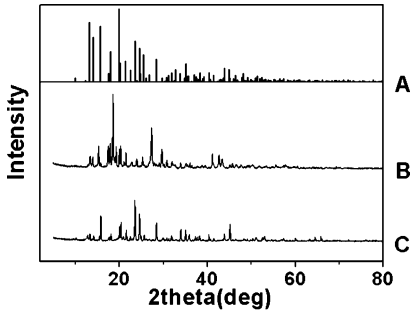

Figure 7. XPRD patterns for **2**: (A) the simulated pattern, (B) taken at room temperature, and (C) after heating at 350 °C for 2 h.

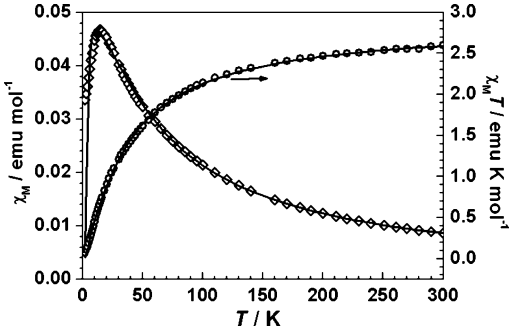

Figure 8. Plots of the temperature dependence (from 300 to 2 K) of $\chi_M T$ and χ_M (solid) in **1** at a field of 1000 G. The magnetic susceptibility was measured using two consecutive cycles, each from 2 to 300 K and back. As no variation was observed, a representative cycle (2−300 K) is shown.

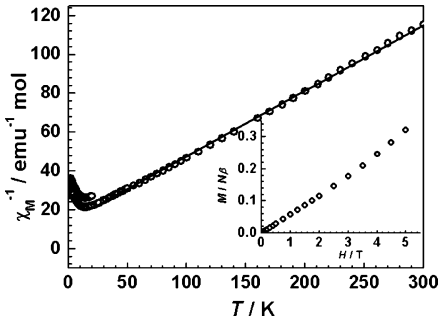

Figure 9. Plot of temperature dependence (from 300 to 2 K) of χ_M^{-1} at a field of 1000 G. The insert is the magnetization curve of **1** at 2 K.

2 h; the position of the most intensive line remain unchanged relative to the simulated diffraction patterns (Figure 7). This experiment also indicates the high thermal stability of **2**.

Magnetic Properties. The magnetic properties of **1** in the form of $\chi_M T$ and χ_M versus T (χ_M being the molar magnetic susceptibility) plots are shown in Figure 8. Data were collected between 2 and 300 K in an applied field of 1000 Oe. The $\chi_M T$ value at room temperature is 2.60 emu K mol^{-1}, higher than the spin-only value of 1.875 emu K mol^{-1} expected for a magnetically isolated Co(II) system with $S = 3/2$. Upon cooling, the $\chi_M T$ values continuously decrease, with a value very close to zero at 2 K. The susceptibility curve shows a broad maximum at 15 K. This behavior suggests the occurrence of a relatively important intrachain antiferromagnetic coupling between the Co(II) ions and the presence of a significant orbital contribution. The temperature dependence of χ_M^{-1} between 300 and 25 K (Figure 9) approximates Curie−Weiss behavior with $C = 2.96$ emu K mol^{-1} and $\theta = -41.2$ K. The negative sign of the Curie−Weiss constant is consistent with the antiferromagnetic interactions between Co(II) centers.

According to the structure of **1**, it could be presumed that the main magnetic interactions between the metal centers might happen between two carboxylate-bridged 1D chains, whereas the superexchange interactions between Co(II) ions through the AIP bridge can be ignored because of the length of the AIP ligands. Because of the spin−orbit coupling contribution of Co(II) ions, it is difficult to find an accurate analytical expression to describe the temperature dependence of the magnetic susceptibility for chains of Co(II) ions. To obtain an estimate of the strength of the antiferromagnetic coupling, we used a simple phenomenological equation proposed by Masciocchi and Rabu,[23] $\chi T = A \exp(-E_1/kT) + B \exp(-E_2/kT)$, to fit the magnetic data of **1**. Here, $A + B$ equals the Curie constant, E_1 and E_2 represent the "activation energy" corresponding to the spin−orbital coupling and the antiferromagnetic exchange interaction, respectively. The least-squares fit (the agreement factor $R = \sum[(\chi_M T)_{obs} - (\chi_M T)_{calcd}]^2/\sum(\chi_M T)_{obs}^2 = 8.2 \times 10^{-4}$) of the experimental data to the above expression led to $A + B = 2.87$ emu K mol^{-1} and $E_1/k = 45.7$ K, in agreement with those given in the literature for the Curie constant and the effect of spin−orbit coupling.[24] The value of $-E_2/k = -9.1$ K, obtained for the antiferromagnetic coupling, is more negative than the values found in coordination polymer chains of the Co(II) ions bridged by the carboxylate in the anti−anti conformations, indicating that a stronger antiferromagnetic exchange interaction is mediated by the double carboxylate bridge in syn−syn conformations.

The molar magnetization data for **1** in the form of M versus H in the field range 0−5 T at 2 K is shown in the inset of Figure 9. The magnetization under 5 T at 2 K is only 0.32 $N\beta$ per Co(II) ion, far from the saturation value of 2.1−2.5 $N\beta$ expected for a Co(II) ions with $S = 1/2$, and $g = 4.1-5$ at low temperature,[25] strongly suggesting antiferromagnetic coupling between Co(II) ions in **1**.

The magnetic properties of **2** in the form of plots of both $\chi_M T$ and χ_M^{-1} versus T are shown in Figure 10. The $\chi_M T$ value per Co(II) at 300 K is 3.1 emu K mol^{-1}, higher than the expected spin-only value for a magnetically isolated Co(II) ion because of the orbit contribution. The $\chi_M T$ value decreases slightly from room temperature to 120 K and then rapidly decreases to 0.45 emu K mol^{-1} at 2 K. The magnetic susceptibility versus T plot exhibits a maximum at 3.5 K under an applied magnetic field of 2000 Oe. All these features indicate an antiferromagnetic coupling in **2** with $T_N = 3.5$ K and a long-range antiferromagnetic order. The 10−300 K temperature dependence of χ_M^{-1} was fit by the Curie−Weiss expression with C values of 3.18 emu K^{-1} mol^{-1} and θ values of −10.8 K. The negative θ values also indicate

(23) Rueff, J.-M.; Masciocchi, N.; Rabu, P.; Sironi, A.; Skoulios, A. *Eur. J. Inorg. Chem.* **2001**, 2843−2848.
(24) (a) Rueff, J. M.; Masciocchi, N.; Rabu, P.; Sironi, A.; Skoulios, A. *Chem.—Eur. J.* **2002**, *8*, 1813. (b) Carlin, R. L. *Magnetochemistry*; Springer-Verlag: Berlin, 1986.
(25) (*a*) Drillon, M.; Coronado, E.; Belaiche, M.; Carlin, R. L. *J. Appl. Phys.* **1988**, *63*, 3551. (*b*) Konar, S.; Mukherjee, P. S.; Zangrando, E.; Floret, F.; Chaudhuri, N. R. *Angew. Chem., Int. Ed.* **2002**, *41*, 1561. (c) Robinson, W. K.; Friedberg, S. A. *Phys. Rev.* **1960**, *117*, 402.

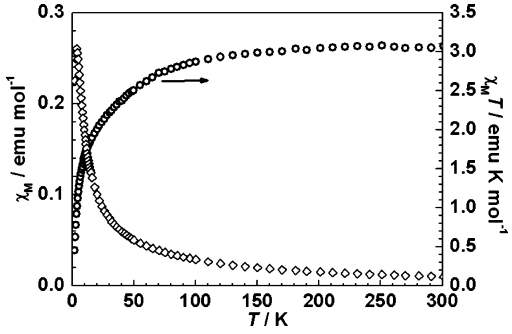

Figure 10. Plots of the temperature dependence (from 300 to 2 K) of $\chi_M T$ and χ_M^{-1} of **2** in a field of 2000 G; the solid line represents the best theoretical fit. The insert is the magnetization curve of 2 at 2 K.

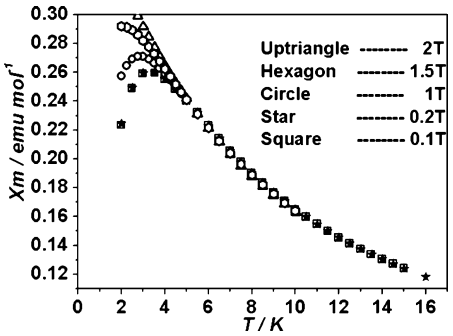

Figure 11. Evolution of the magnetic susceptibility of **2** as a function of the temperature, measured on cooling under an external magnetic field (2, 1.5, 1T, 0.2, and 0.1 T, from top to bottom in the plot) as noted on the graph.

antiferromagnetic coupling between the metal sites. Considering that the Co···Co distance (4.3 Å) within the $Co_2(CO_2)_2$ SUB is much shorter than those for interdimer distances (6.05 and 8.86 Å), the observed antiferromagnetic interaction should mainly arise from the exchange between the magnetic centers within Co2 dimers. The susceptibility data were thus approximately analyzed by an isotropic dimer mode of spin $S = 3/2$;[26] fitting the experimental data above 30 K gave $J = -1.33$ cm^{-1}, $g = 2.77$, and $R = 8.04 \times 10^{-5}$. It is interesting to note that the susceptibility maximum of **2** depends on the magnitude of the applied magnetic field (H). A broadening of this maximum is observed as long as the field is increased, and it disappears when the applied field is greater than 2 T (Figure 11), suggesting the occurrence of a field-induced magnetic transition.

The field-dependent magnetization of **2** at 2 K has an S-shaped curve, indicating the occurrence of a magnetic transition from the antiferromagnetic ground state to a spin-polarized state.[27] The critical field, determined by the dM/dH curve, is ca. 2 T at 2 K, consistent with the observations of temperature-dependent magnetic susceptibilities under different applied fields (Figure 12). The magnetization at 5 T is 2.27 $N\beta$, close to the saturation value of ca. 2.3 $N\beta$ expected for a Co(II) ion with $S = 1/2$ and $g = 4.6$.[28]

In the structure of **2**, the double-carboxylate-bridged dinuclear Co(II) units are connected by AIP spacers to form

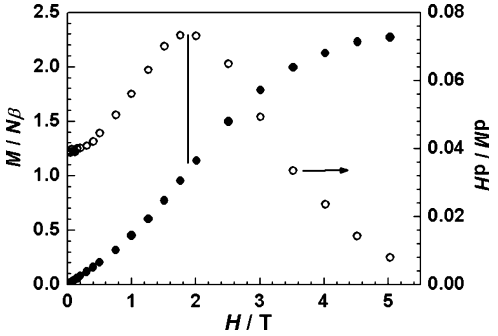

Figure 12. Plots of the field-dependent magnetization of **2** at 2 K with the critical field being ca. 2 T.

an extended 3D framework. As the Co···Co distance over the carboxylate bridge (4.3 Å) is much shorter than those over the AIP spacers (6.05−8.86 Å), the exchange coupling through the carboxylate bridge should be dominant. The field-induced magnetic transition in **2** is similar to some observations in metal phosphonates containing dimer units in ladderlike chain structures; the critical field is slightly less than those found in Co(II) phosphonates despite a larger M···M distance (4.3 Å) relative to the M−O−M bond angle.[27,29] As a comparison, the magnetic behavior of the dehydrated product of **2** has been performed and the value of T_N remained, together with the same S-shaped curve, in field-dependent magnetization of **2** at 2 K. (See Figures S1 and S2 in the Supporting Information.)

Conclusion

Two novel, highly stable supramolecular complexes have been synthesized. The structural and thermal characterization of both display stable microporous 3D open frameworks. The water molecules, acting as the guest molecules in **1** and as the disguise guest molecules (which occupied the pore in the architecture by coordinating to the metal and could be removed easily like the guest molecules) in **2**, are distinct in these two complexes. The behavior of both polymers **1** and **2** corresponds to an antiferromagnetically coupled system, and field-induced magnetic transition is observed in **2**. Upon liberating coordinated H_2O molecules, complex **2** has interesting coordination-unsaturated Co sites. These works reveal that the solvents and the pH value play very important roles in the formation of different coordination frameworks, and this offers the possibility of controlling the formation of such network structures by varying those factors.

Acknowledgment. This work was supported by the National Natural Science Foundation of China under Project 20173063, the State Key Basic Research and Development Plan of China (001CB108906), and the NSF of Fujian Province (E0020001).

Supporting Information Available: Plots of the magnetic behavior of dehydrated **2** (pdf) and crystallographic information data for **1** and **2** (cif). This material is available free of charge via the Internet at http://pubs.acs.org.

IC0602244

(26) Liu, Y. H.; Tsai, H. L.; Lu, Y. L.; Wen, Y. S.; Wang, J. C.; Lu, K. L. *Inorg. Chem.* **2001**, *40*, 6426.
(27) Zheng, L.-M.; Gao, S.; Yin, P.; Xin, X.-Q. *Inorg. Chem.* **2004**, *43*, 2151.
(28) Caneschi, A.; Dei, A.; Gatteschi, D.; Tangoulis, V. *Inorg. Chem.* **2002**, *41*, 3508.
(29) Yin, P.; Gao, S.; Wang, Zh.-M.; Yan, Ch.-H.; Zheng, L.-M.; Xin, X.-Q. *Inorg. Chem.* **2005**, *44*, 2761.